

pp Elastic Scattering at LHC and Nucleon Structure (Conference Report)¹

M. M. Islam*, R. J. Luddy* and A. V. Prokudin[†]

*Department of Physics, University of Connecticut, USA

[†]Department of Theoretical Physics, University of Torino and INFN, Torino, Italy

Abstract. High energy elastic pp differential cross section at LHC at the c.m. energy 14 TeV is predicted using the asymptotic behavior of $\sigma_{tot}(s)$ and $\rho(s)$, and the measured $\bar{p}p$ differential cross section at $\sqrt{s} = 546$ GeV. The phenomenological investigation has progressively led to an effective field theory model that describes the nucleon as a chiral bag embedded in a quark-antiquark condensed ground state. The measurement of pp elastic scattering at LHC up to large $|t| \gtrsim 10$ GeV² by the TOTEM group will be crucial to test this structure of the nucleon.

High energy pp and $\bar{p}p$ elastic scattering have been measured at the CERN ISR[1] and SPS Collider[2-3] over a wide range of energy and momentum transfer: $\sqrt{s} = 23$ -630 GeV and $|t| = 0$ -10 GeV². These measurements have been followed by Fermilab Tevatron measurement[4-5] of $\bar{p}p$ at $\sqrt{s} = 1.8$ TeV and $|t| = 0$ -0.5 GeV². Such a large experimental effort naturally presents us with the following questions:

1. What do we learn from these experiments about NN interactions at high energies?
2. What insight do we get from them about the physical structure of the nucleon?

These questions have now assumed greater significance because of the Large Hadron Collider (LHC) currently being built at CERN. One of the first experiments planned at LHC called TOTEM (Total and Elastic Measurement) will measure pp elastic $\frac{d\sigma}{dt}$ in the near forward direction at an unprecedented c.m. energy $\sqrt{s} = 14$ TeV.

My collaborators and I have been studying high energy pp , $\bar{p}p$ elastic scattering for some time[6-8]. Our initial phenomenological investigation led us to the following description. The nucleon has an outer cloud and an inner core (Fig. 1). High energy elastic scattering is primarily due to two processes (Fig. 2): 1) a glancing collision where the outer cloud of one nucleon interacts with that of the other giving rise to diffraction scattering; 2) a hard (or large $|t|$) collision where one nucleon core scatters off the other core via vector meson ω exchange, while their outer clouds overlap and interact independently. In the small $|t|$ region diffraction dominates, but the hard scattering takes over as $|t|$ increases.

Let me present an example from our recent calculations. The solid curve in Fig. 3 is our calculated $\frac{d\sigma}{dt}$ for $\bar{p}p$ scattering at $\sqrt{s} = 546$ GeV. The dotted curve is the differential cross section due to diffraction alone, while the dot-dashed curve is that due to the hard

¹ Presented by M. M. Islam at the Conf. on Intersections of Particle and Nuclear Physics (N.Y., May 2003), the 8th Int. Wigner Symposium (CUNY, N.Y., May 2003) and the 10th Blois Workshop (Helsinki, June 2003). Details of the paper have appeared in: Mod. Phys. Lett. 18(2003)743; hep-ph/0210437.

scattering alone. As we can see, diffraction dominates in the small $|t|$ region, but falls off rapidly as $|t|$ increases, and the hard scattering takes over. The interference between the diffraction and the hard scattering produces the dip. The experimental data are from SPS Collider[2]. The thick dashed curve in Fig. 3 is our calculated pp elastic $\frac{d\sigma}{dt}$ at $\sqrt{s} = 500$ GeV, which is currently being measured at RHIC in the small $|t|$ region[9].

We describe diffraction scattering using the impact parameter representation:

$$T_D(s, t) = i p W \int_0^\infty b db J_0(bq) \Gamma_D(s, b); \quad (1)$$

q is the momentum transfer ($q = \sqrt{|t|}$) and $\Gamma_D(s, b)$ is the profile function, which is related to the eikonal function $\chi_D(s, b)$: $\Gamma_D(s, b) = 1 - \exp(i\chi_D(s, b))$. We take $\Gamma_D(s, b)$ to be an even Fermi profile function:

$$\Gamma_D(s, b) = g(s) \left[\frac{1}{1 + \exp((b-R)/a)} + \frac{1}{1 + \exp(-(b+R)/a)} - 1 \right]. \quad (2)$$

The parameters R and a are energy dependent: $R = R_0 + R_1(\ln s - \frac{i\pi}{2})$, $a = a_0 + a_1(\ln s - \frac{i\pi}{2})$; $g(s)$ is a complex crossing even energy-dependent coupling strength.

Our hard scattering amplitude is of the form

$$T_H(s, t) \sim \exp[i\chi_D(s, 0)] s \frac{F^2(t)}{m_\omega^2 - t}. \quad (3)$$

The t -dependence is the product of two form factors and the ω propagator. It shows that ω probes two density distributions corresponding to the two form factors. The density distributions represent the nucleon cores. The factor of s originates from spin 1 of ω . The factor $e^{i\chi_D(s, 0)}$ represents absorptive correction due to diffraction scattering. The diffraction amplitude obtained by us satisfies a number of general properties associated with the phenomenon of diffraction:

1. $\sigma_{tot}(s) \sim (a_0 + a_1 \ln s)^2$ (Froissart-Martin bound)
2. $\rho(s) \simeq \frac{\pi a_1}{a_0 + a_1 \ln s}$ (derivative dispersion relation)
3. $T_D(s, t) \sim i s \ln^2 s f(|t| \ln^2 s)$ (AKM scaling)
4. $T_D^{\bar{p}p}(s, t) = T_D^{pp}(s, t)$ (crossing even)

Our present approach is different from our earlier one[8], where we fitted known $\frac{d\sigma}{dt}$ at different energies using complex energy-dependent parameters. Our goal now is to obtain the asymptotic behavior and the approach to the asymptotic behavior of the elastic scattering amplitude, so that we can predict the pp differential cross section at $\sqrt{s} = 14$ TeV. To this end, we require the energy-dependent parameters to describe quantitatively the asymptotic behavior and the approach to the asymptotic behavior of total cross section $\sigma_{tot}(s)$ and $\rho(s) = \frac{ReT(s, 0)}{ImT(s, 0)}$ as known from dispersion relation calculations. Furthermore, we require them to describe well the measured $\bar{p}p$ elastic differential cross section at 546 GeV[2]. Here are the results of our calculations of $\sigma_{tot}(s)$ (Fig. 4), $\rho(s)$ (Fig. 5), and $\frac{d\sigma}{dt}$ at $\sqrt{s} = 546$ GeV (Fig. 3) shown earlier. We find a satisfactory description. Once the parameters are determined, we can test our model by predicting $\frac{d\sigma}{dt}$ at higher energies where experimental data are available. Fig. 6 shows our prediction at $\sqrt{s} = 1.8$ TeV for $\bar{p}p$ compared with the Tevatron data[4-5]. Fig. 7 shows our prediction for $\bar{p}p$ elastic scattering at $\sqrt{s} = 630$ GeV, where large $|t|$ data are available from SPS Collider[3]. These tests indicate that the model provides a reasonably quantitative description of high energy elastic scattering.

We now proceed to predict pp elastic $\frac{d\sigma}{dt}$ at LHC at the c.m. energy 14 TeV (Fig. 8). The solid curve is our predicted differential cross section. The dashed curve represents the prediction by the impact-picture model of Bourrely et al. and the dot-dashed curve represents that by the Regge pole-cut model of Desgrolard et al.[10-13]. The latter models predict typical diffraction oscillations in the large $|t|$ region, while our model predicts smooth fall-off of $\frac{d\sigma}{dt}$ for $|t| > 1.5 \text{ GeV}^2$. The dotted line in Fig. 8 represents schematically the expected change in our model in the behavior of $\frac{d\sigma}{dt}$ from Orear fall-off: $\frac{d\sigma}{dt} \sim e^{-a\sqrt{|t|}}$ to a power fall-off: $\frac{d\sigma}{dt} \sim t^{-10}$ due to quark-quark scattering.

Our phenomenological investigation progressively led us to an effective field theory model that describes the nucleon structure. This development began with a criticism of our model which was the following: The hard scattering amplitude in our model (Eq.(3)) has a factor of s from spin 1 of ω , and the s and t dependence of this amplitude shows that ω behaves as an elementary vector meson. On the other hand, at such high energies one would expect ω to Reggeize and s be replaced by $s^{\alpha_\omega(t)}$, where $\alpha_\omega(t)$ is the ω trajectory. $\alpha_\omega(t)$ is considerably less than 1 at large $|t|$ and therefore this amplitude should give negligible contribution contrary to our calculations. However, we noticed that in the non-linear σ -model of the nucleon, ω couples to the baryonic current like a gauge boson: $g\omega_\mu J_B^\mu$, and the baryonic current is topological:

$$J_B^\mu = \frac{\varepsilon^{\mu\nu\rho\sigma}}{24\pi^2} \text{tr}[U^\dagger \partial_\nu U U^\dagger \partial_\rho U U^\dagger \partial_\sigma U] \quad (4)$$

What this model says is that it is an effective field theory model. But, as long as it holds, baryonic current continues to behave as a topological current and ω coupled to it as a gauge boson continues to behave as a gauge boson, i.e. as an elementary vector meson. And we seem to be seeing this behavior.

Fortunately, there was a way of testing this conclusion. From our ωNN form factor $F(t)$, we can obtain by Fourier transform the baryonic charge distribution and then derive the pion field that gives rise to this baryonic charge distribution. We can compare this pion field with the pion field obtained in the n.l. σ -model, which describes the nucleon as a topological soliton or Skyrmion. Here is the result of our analysis: Fig. 9. The solid curve is our calculated pion field configuration, or pion profile function $\theta(r)$, while the dotted and the dashed curves are the pion profile functions from the n.l. σ -model. The curves are consistent with each other, if we bear in mind that our curve is coming from c.m. energy region $\gtrsim 23 \text{ GeV}$, while the other curves are coming from an energy region of order 1 GeV. Furthermore, the r.m.s. radius for the baryonic charge distribution obtained by us is 0.44 F, while that from the n.l. σ -model is about 0.5 F.

We faced another problem at this point. Even though the n.l. σ -model when gauged describes the low energy properties of the nucleon quite well, it typically predicts a soliton mass $m_{sol} \sim 1500 \text{ MeV}$ compared to the nucleon mass $m_N = 939 \text{ MeV}$ (see, for example,[14]). We obviously had to confront this problem of large soliton mass as we were claiming evidence in favor of the soliton model. To this end, we examined a model more general than the n.l. σ -model. The model turns out to be the linear σ -model of Gell-Mann and Levy, which is described by the Lagrangian:

$$\mathcal{L} = \bar{\psi} i \gamma^\mu \partial_\mu \psi + \frac{1}{2} (\partial_\mu \sigma \partial^\mu \sigma + \partial_\mu \vec{\pi} \partial^\mu \vec{\pi}) - g \bar{\psi} [\sigma + i \vec{\tau} \cdot \vec{\pi} \gamma^5] \psi - \lambda (\sigma^2 + \vec{\pi}^2 - f_\pi^2)^2. \quad (5)$$

The model has $SU(2)_L \times SU(2)_R \times U(1)_V$ global symmetry and spontaneous breakdown of chiral symmetry. ψ is the quark field, σ is an isospin-zero scalar field,

and $\vec{\pi}$ is an isovector pseudoscalar field. The model can be expressed in terms of right and left quark fields $\psi_{R,L} = \frac{1}{2}(1 \pm \gamma^5)\psi$ by introducing a scalar field ζ and a unitary field U in the following way: $\sigma + i\vec{\tau} \cdot \vec{\pi} = \zeta U$, $\zeta = \sqrt{\sigma^2 + \vec{\pi}^2}$, $U = e^{\frac{i\vec{\tau} \cdot \vec{\phi}}{f_\pi}}$.

The field $\vec{\phi}$ is the massless Goldstone pion field; U is the Skyrmion field that gives rise to the topological baryonic current. In terms of these fields, Eq.(5) takes the form

$$\begin{aligned} \mathcal{L} = & \bar{\psi}_R i \gamma^\mu \partial_\mu \psi_R + \bar{\psi}_L i \gamma^\mu \partial_\mu \psi_L + \frac{1}{2} \partial_\mu \zeta \partial^\mu \zeta + \frac{1}{4} \zeta^2 \text{tr}[\partial_\mu U \partial^\mu U^\dagger] \\ & - g \zeta (\bar{\psi}_L U \psi_R + \bar{\psi}_R U^\dagger \psi_L) - \lambda (\zeta^2 - f_\pi^2)^2. \end{aligned} \quad (6)$$

In the conventional n.l. σ -model, one replaces from the very beginning the scalar field ζ by its vacuum value f_π . Furthermore, one introduces a Weiss-Zumino-Witten anomalous action term[15], which arises from the underlying quark structure of the model. It is this action that contains the term $g\omega_\mu J_B^\mu$, which couples ω to the topological baryonic current. The n.l. σ -model also assumes that all the important low-energy interactions are in the meson sector. The only important interaction coming from the quark sector is that given by the WZW action and no further interaction in the quark sector needs to be included. This, of course, leads to a Skyrmion lying in a non-interacting Dirac sea (Fig. 10). On the other hand, we notice from the linear σ -model that even though replacing ζ by its vacuum value f_π may be reasonable in the meson sector, completely neglecting it in the quark sector is questionable, because the ζ field provides an interaction between left and right quarks (Eq.(6)). The latter makes the quarks massive and leads to the spontaneous breakdown of chiral symmetry. This, of course, means that we have a soliton lying in an interacting Dirac sea (Fig. 10). What one finds is that if the scalar field has a critical behavior, and by this I mean a scalar field that is zero for small distances, but rises sharply at some distance R to its vacuum value f_π (Fig. 11), then the energy of the interacting Dirac sea together with that of the scalar field is considerably less than that of the non-interacting Dirac sea[16]. The system therefore makes a transition to this lower ground state and significantly reduces its total energy or mass. This condensation phenomenon solves the soliton mass problem and is analogous to superconductivity. Instead of spin up and down electrons, we have left and right quarks forming a $q\bar{q}$ condensate.

The behavior of the ζ field shown in Fig. 11 has significant implications. First, for $r < R$, $\zeta = 0$ — quarks are massless, and we are in a perturbative regime. Therefore, we end up with the nonperturbative structure of the nucleon shown in Fig. 12, which shows that the nucleon is a chiral bag[15,17] embedded in a $q\bar{q}$ condensed ground state. Second, for momentum transfer $Q = \sqrt{|t|}$ sufficiently large, one nucleon probes the other nucleon at an impact parameter $b \approx \frac{1}{Q} < R$, and therefore in the perturbative regime where pp elastic scattering originates from valence quark-quark scattering. The latter has been investigated by Sotiropoulos and Sterman[18] who concluded that at very large $|t|$, $\frac{d\sigma}{dt} \sim t^{-10}$ (same as power counting rules). From our point of view, this means that as momentum transfer Q increases, there will be a critical value $Q_0 \approx \frac{1}{R}$ beyond which $\frac{d\sigma}{dt}$ will tend to a power fall-off. Schematically, the dotted line in Fig. 8 represents this transition from the nonperturbative regime to the perturbative regime and, in fact, will be a signature of the chiral phase transition.

Concluding remarks

1. Our phenomenological investigation has led us to physical aspects of the nucleon which have been proposed and studied by other authors in different contexts.
2. We find that the nucleon is a chiral bag embedded in a quark-antiquark ground state, and this ground state is analogous to a superconducting ground state. We also find that this structure is described by an effective field theory model — a gauged Gell-Mann-Levy linear σ -model.
3. The experimental study of pp elastic scattering at LHC at $\sqrt{s} = 14$ TeV by the TOTEM group up to large $|t|$ will be crucial to test this structure of the nucleon.

REFERENCES

1. Nagy, E., et al., *Nucl. Phys.*, **B150**, 221 (1979).
2. Bozzo, M., et al., *Phys. Lett.*, **B147**, 385 (1984); **B155**, 197 (1985).
3. Bernard, D., et al., *Phys. Lett.*, **B171**, 142 (1986).
4. Amos, N., et al., *Phys. Lett.*, **B247**, 127 (1990).
5. Abe, F., et al., *Phys. Rev.*, **D50**, 5518 (1994).
6. Heines, G. W., and Islam, M. M., *Nuovo Cimento*, **61A**, 149 (1981).
7. Islam, M. M., Fearnley, T., and Guillaud, J. P., *Nuovo Cimento*, **81A**, 737 (1984).
8. Islam, M. M., Innocente, V., Fearnley, T., and Sanguinetti, G., *Europhys. Lett.*, **4**, 189 (1987).
9. Guryn, W., *Nucl. Phys. (Proc. Suppl.)*, **B99**, 299 (2001).
10. Bourrely, C., Soffer, J., and Wu, T. T., *Phys. Rev. Lett.*, **54**, 757 (1985).
11. Bourrely, C., et al., “Quarter Century of Rising Total Cross Sections,” in *Frontiers in Strong Interactions*, edited by P. Chiappetta, M. Haguenaue, and J. T. T. Van, Editions Frontieres, 1996, p.15.
12. Desgrolard, P., Giffon, M., and Predazzi, E., *Z. Phys.*, **C63**, 241 (1994).
13. Buenerd, M., “The TOTEM project at LHC,” in *Frontiers in Strong Interactions*, edited by P. Chiappetta, M. Haguenaue, and J. T. T. Van, Editions Frontieres, 1996, p.437.
14. Zhang, L., and Mukhopadhyay, N. C., *Phys. Rev.*, **D50**, 4668 (1994).
15. Bhaduri, R. K., *Models of the Nucleon: from Quarks to Soliton*, Addison-Wesley, Reading, Massachusetts, 1988.
16. Islam, M. M., *Z. Phys.*, **C53**, 253 (1992).
17. Hosaka, A., and Toki, H., *Quarks, Baryons, and Chiral Symmetry*, World Scientific, 2001.
18. Sotiropoulos, M. G., and Sterman, G., *Nucl. Phys.*, **B425**, 489 (1994).

Figures 1 - 12: Explanations of the figures are given in the main body of the paper.

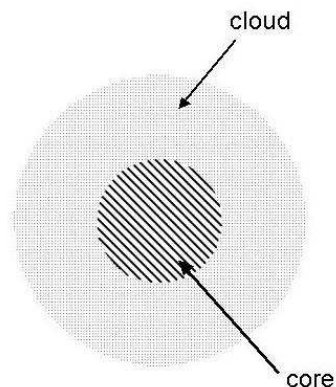


FIGURE 1.

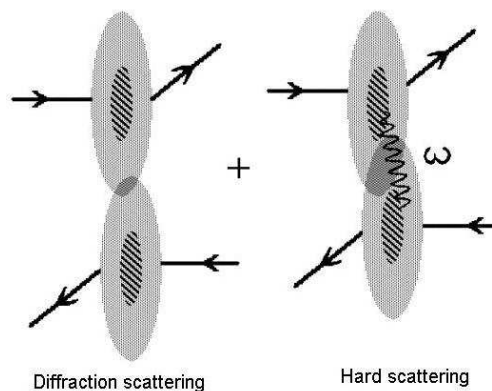


FIGURE 2.

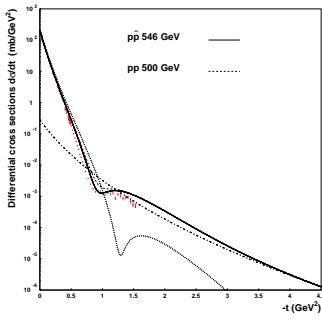


FIGURE 3.

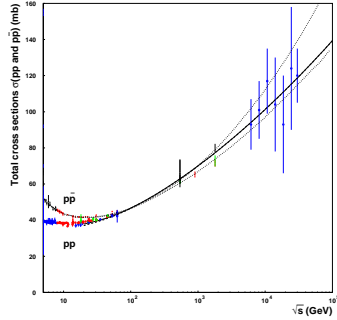


FIGURE 4.

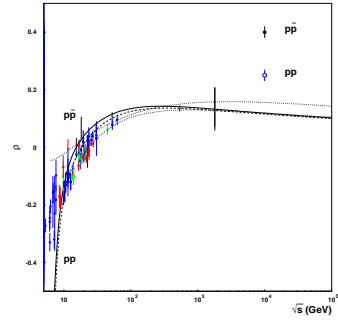


FIGURE 5.

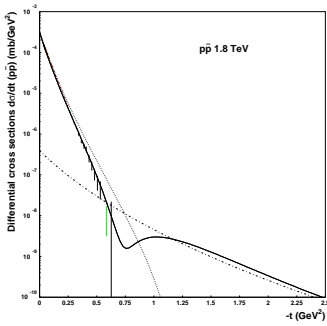


FIGURE 6.

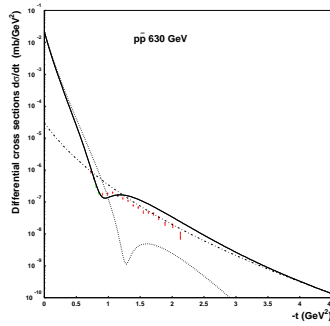


FIGURE 7.

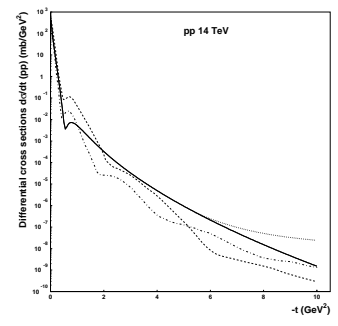


FIGURE 8.

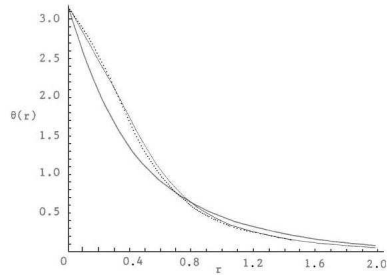


FIGURE 9.

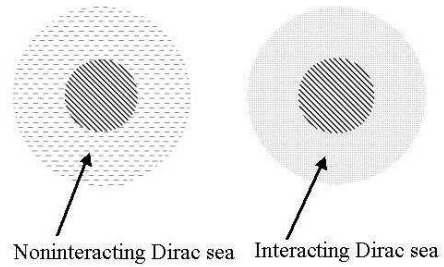


FIGURE 10.

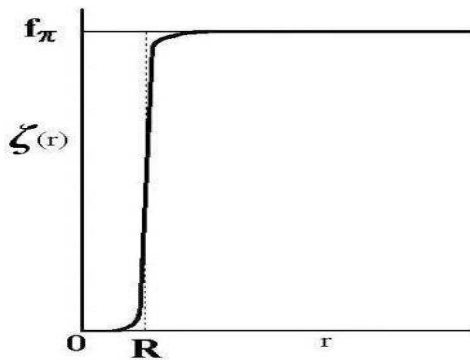


FIGURE 11.

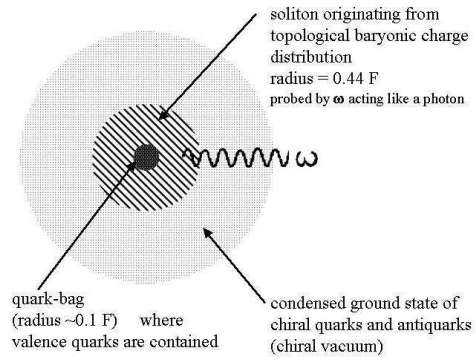


FIGURE 12.